Photonic crystal Mach-Zehnder interferometer operating in the self-collimation mode of light

Hoang M. Nguyen, E.W.J.M. van der Drift, J. Caro, S. Rogge and H.W.M. Salemink
Kavli Institute of Nanoscience, Delft University of Technology, The Netherlands
Lorentzweg 1, 2628 CJ, Delft, The Netherlands

ABSTRACT

Based on the self-collimation effect of light propagating inside a photonic crystal, we demonstrate a novel concept for a compact Mach-Zehnder interferometer. The properties of these self-collimated beams are such that we can manipulate them to form the beam splitters and mirrors of the Mach-Zehnder interferometer in a very compact area of 20x20 μm^2. We obtain the unidirectional output behaviour characterized by the high contrast in the telecommunication-wavelength signal at the two outputs of the photonic crystal Mach-Zehnder interferometer. The experiments are done using optical transmission spectroscopy and far-field optical microscopy. This photonic crystal Mach-Zehnder interferometer holds a promise for a compact Mach-Zehnder modulator, inspired by recent reports of NEMS-based photonic crystal membrane.

Keywords: photonic crystal, self-collimation, MZI, modulator

1. INTRODUCTION

Optical interconnects based on silicon-on-insulator (SOI) and fabricated with CMOS compatible fabrication technology will likely replace the electrical one for high data rate circuits [1-3]. Among early optical devices, the high speed Mach-Zehnder modulator (MZM) based on silicon waveguides [2] is promising for telecommunication networks. However, owing to the requirement for sufficient phase shift between the two MZM arms, its millimeter-scale dimensions [2] are still a significant disadvantage for integration within microprocessors [3]. Therefore, much effort is being made to miniaturize these modulators without sacrificing their sufficient phase shift, particularly engineering the MZM arms with slow-light structures [3-5]. Here, we demonstrate a different approach to realize the first ultra-compact silicon photonic crystal (PhC) Mach-Zehnder interferometer (MZI) operating in the self-collimation mode of light. Our approach proposes a compact optical silicon modulator, where the differential output signal could be tuned by varying refractive index locally at the beam splitter's air holes instead of along one of the MZI arms.

1.1 Self-collimation effect in a photonic crystal

Self-collimation of light propagation in a PhC structure is a unique phenomenon, where light at specific wavelengths travels in a particular direction with almost no diffraction. This phenomenon originates from the flat section of the strongly anisotropic equi-frequency contours (EFCs) of the PhC structures within defined frequency ranges. As energy propagates along the direction normal to the EFCs, a light beam is collimated once its frequency reaches the level of the square EFCs and its wave vector is limited to within the ultra-flat region (between light and dark orange regions shown in the zoomed-area of figure 1a). The collimation effect in PhC is of increasing interest, both in terms of theoretical and practical research [6-8]. Although simple elements such as beam splitters and mirrors utilizing the collimated light have been realized [9-12]; a PhC MZI has not yet been demonstrated experimentally.

Photonic and Phononic Crystal Materials and Devices X, edited by Ali Adibi, Shawn-Yu Lin, Axel Scherer,
Proc. of SPIE Vol. 7609, 76090P · © 2010 SPIE · CCC code: 0277-786X/10/$18 · doi: 10.1117/12.841701

Downloaded from SPIE Digital Library on 19 Mar 2010 to 131.180.130.114. Terms of Use: http://spiedl.org/terms

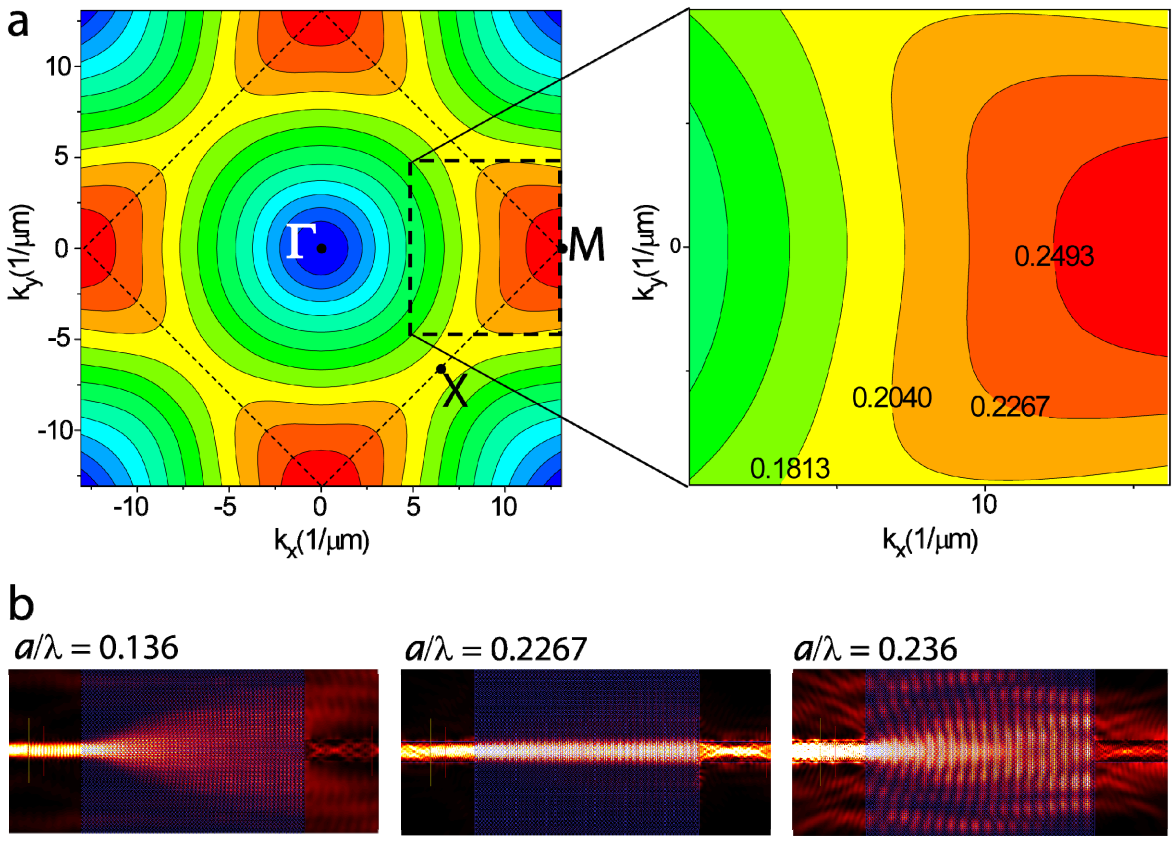


Figure 1. 1a, Equi-frequency contours diagram for the lowest TE-mode energy band of the square lattice PhC is plotted up to the second Brillouin zone. The colours correspond to normalized energy levels a/λ. The blue and green regions are isotropic dispersion regions, where TE light at these frequencies are normally diffracted by the PhC. The yellow and red dispersion regions (a/λ from 0.1813 to 0.2493) are strongly anisotropic, resulting in collimation and negative refractive index phenomena. The square EFC at a/λ = 0.2267, between the light and dark orange regions, is the origin of the collimated light propagation. 1b, finite-element frequency-domain (FEFD) simulations illustrating light propagation through the PhC from the input waveguide to the output waveguide, in the self-collimation mode at a/λ = 0.136 and in the diffraction modes at a/λ = 0.2267 and a/λ = 0.236.

2. DESIGN OF THE PHOTONIC CRYSTAL MACH-ZEHNDER INTERFEROMETER

The PhC platform that we use for the MZI is two-dimensional (2D), formed by a square lattice of air holes in a 220 nm thick layer of SOI (see figure 2). This slab-type structure provides a strong vertical confinement of light in silicon due to the large index contrast between the silicon and the air/SiO_2 cladding layer. The lattice constant is a = 340 nm and hole radius is r = 105 nm. Using CrystalWave we calculate the dielectric band of transverse electric (TE) polarized modes of light injected into the PhC under study. The EFC diagram of this band is plot in figure 1a. The refractive indices used for these calculations are $n_{silicon}$ = 3.5 and n_{SiO2} = 1.46. This results in square EFCs at normalized frequencies around a/λ = 0.2267, with the ultra-flat region perpendicular to the ΓM direction. Hence TE-polarized modes of light at free-space wavelength around 1.5 μm are self-collimated as it propagates in the ΓM direction (figure 1b).

A symmetric MZI structure is built on the above 2D PhC platform, consisting of two inputs, two outputs, two 90° beam splitters (S1, S2) and two 90° mirrors (M1, M2), see figure 2. The beam splitter is a single line defect containing larger radius air holes (r_{BS} = 155 nm) compared to those of the PhC platform. The mirror is a smooth PhC-air interface, which behaves as the total internal reflection mirror. The distance between a beam splitter and a mirror along the ΓM direction is 20 unit cells (≈9.6 μm), which ensures a compact total size of the PhC MZI within 20×20 μm^2. Beam splitters and mir-

Downloaded from SPIE Digital Library on 19 Mar 2010 to 131.180.130.114. Terms of Use: http://spiedl.org/terms

rors are oriented along the ΓX direction and are parallel to each other, splitting and reflecting the collimated beam in the ΓM direction. The light beam entering the MZI from the input waveguide IN1 is split equally into two beams at the beam splitter S1. Each of them follows a different symmetric path and is reflected by M1 and M2, respectively. The beam in the S1M2S2 branch has a phase lag of $-\pi/2$ relative to the one in the S1M1S2 branch. The two beams then join at S2, where each of them is split once again and interfere with each other. Finally, the transmitted beams are collected at output waveguides OUT1 and OUT2. For the splitting of the S1M1S2 incident beam, there is a phase shift of $-\pi/2$ between the exiting light beams at OUT1 and OUT2. Analogously, the phase shift is $\pi/2$ for the S1M2S2 branch. As a result of the splitting and phase shift at S1 and S2, there are always two super-positions of two in-phase beams at OUT1 and two out-of-phase beams at OUT2. Therefore, the output beam at OUT1 experiences constructive interference, whereas the interference at OUT2 is destructive [13]. This is called unidirectional output behaviour and was simulated by Zhao et al. [14] with the dielectric-rods-in-air PhC structure. Inset 2 of figure 2 shows 2D finite-element frequency-domain (FEFD) simulation for the propagation of the 1.5 μm TE-polarized light in the PhC MZI studied here. Its unidirectional output behaviour is illustrated in the high and low intensities at the output waveguides OUT1 and OUT2, respectively.

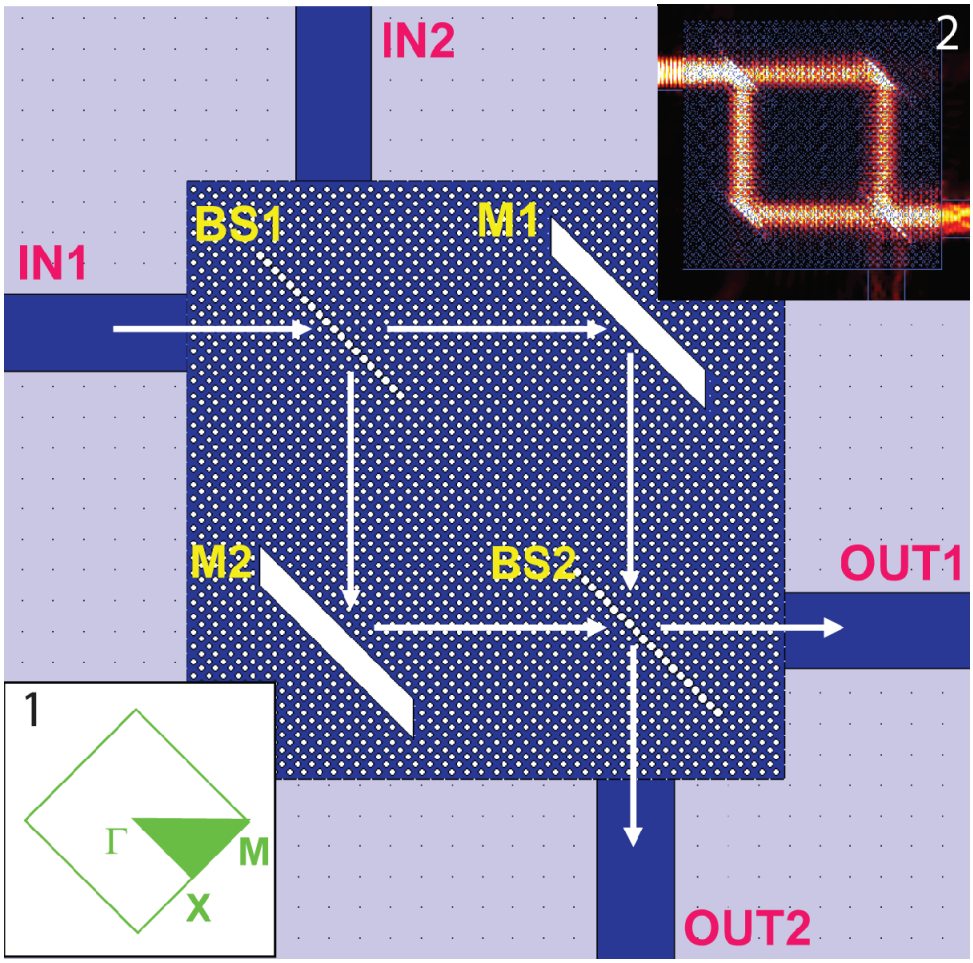


Figure 2. Design of the PhC MZI. Beam splitters S1, S2 are single arrays of holes with radius r = 155 nm. Mirrors M1, M2 are flat air regions in the size of three hole arrays. IN1, OUT1 and OUT2 are input and output waveguides for light coupling to the MZI structure. White arrows indicate light propagation. Inset 1 shows the first Brillouin zone showing the orientation of the PhC. Inset 2 shows a 2D FEFD simulation demonstrating the unidirectional output behaviour of the PhC MZI.

Downloaded from SPIE Digital Library on 19 Mar 2010 to 131.180.130.114. Terms of Use: http://spiedl.org/terms

3. DEVICE FABRICATION

The main fabrication steps of the MZI are electron beam lithography and cryogenic inductively coupled plasma (ICP) etching. A 120 nm thick ZEP resist layer is directly spin-coated onto the SOI chip. For patterns writing we use a Leica 5000+ electron beam pattern generator. The complete MZI pattern including ridge waveguides is written in a single writing step. After resist development, the pattern is transferred to the silicon device layer using ICP etching in a SF_6/O_2 plasma at a substrate temperature of -120°C. The remaining resist is then stripped in PRS3000 at 75°C for 1 hour. Finally, the sample is cleaved perpendicularly through the waveguides to form waveguide facets.

In practice, during sample fabrication and evaluation, we noticed that it is non-trivial to fabricate this MZI with high optical performance. There are two critical issues regarding the fabrication. First, the fabricated MZI substructures must have identical dimensions as designed in order to deliver the simulated unidirectional output behaviour. The most crucial and hard-to-fabricate substructures are the beam splitters, which play a similar role as conventional waveguide couplers [13]. Any small deviation from the design would lead to decay in the optical performance. For instance, the 30 nm narrow silicon veins between the beam splitters' air holes (inset of figure 3) would be opened, leading to insufficient phase shifts, loss, unequal splitting or even mirror-like operation. Second, the circular air holes must be uniform, smooth and vertical at the side wall in order to maintain the collimation effect throughout the device. Despite the above fabrication challenges, we have succeeded in obtaining a high quality PhC-MZI (figure 3) using a simple process flow and observed its superior optical performance.

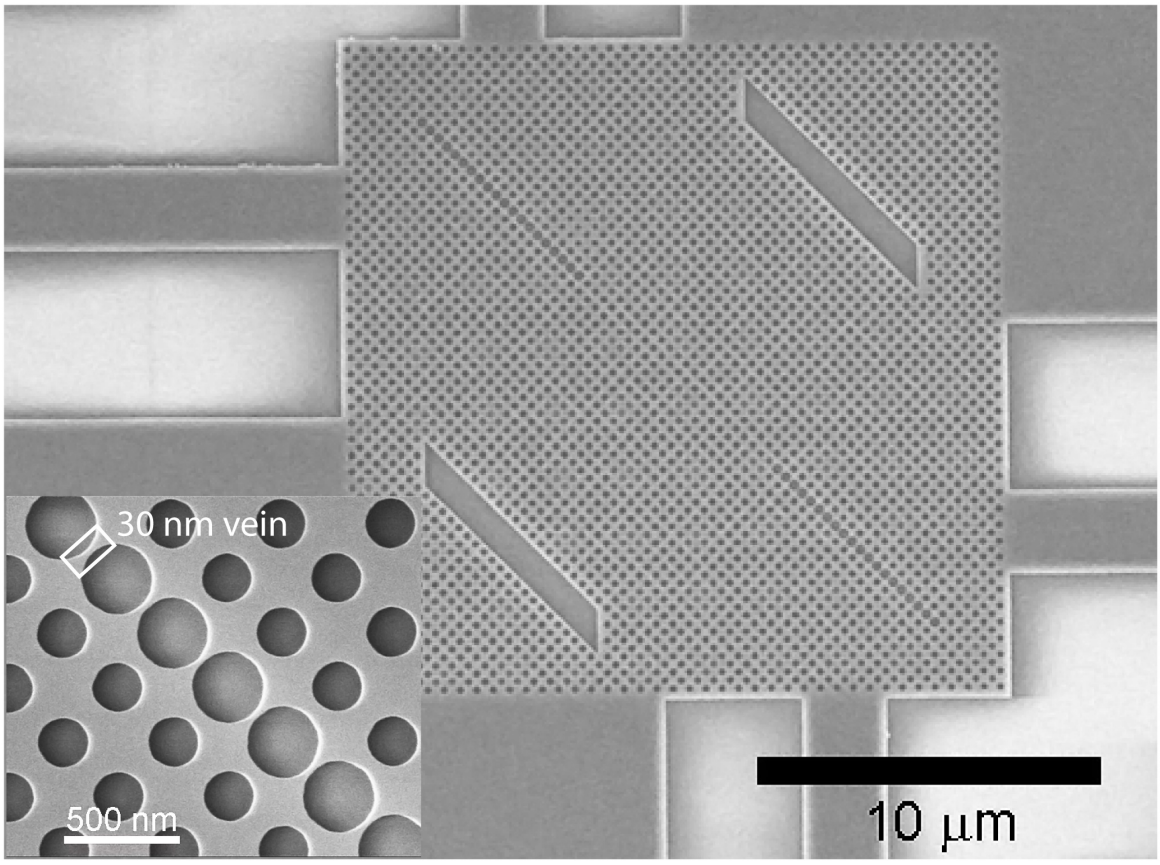


Figure 3. SEM image of the PhC MZI, demonstrating accurate realization of the design. All structures (PhC holes, beam splitters, mirrors and waveguides) are etched in a single etching step. The inset is an SEM image of a beam splitter, featuring smooth circular holes. The hole radius for the regular PhC is $r \approx 105$ nm, while for the line defect it is $r_{BS} \approx 155$ nm, consistent with the design. A narrow vein of a beam splitter is highlighted in the white rectangle.

Downloaded from SPIE Digital Library on 19 Mar 2010 to 131.180.130.114. Terms of Use: http://spiedl.org/terms

4. SIMULATIONS AND MEASUREMENTS

4.1. Transmission simulations and measurements

In figure 4 we present optical transmission measurements obtained with the end-fire technique [15]. The measurements are driven by a tunable near-infrared laser (Santec TSL-210VF, 1.44-1.63 μm). Waveguide facets are used for in- and out-coupling of light and the spatial filter with a 25 μm diameter pinhole is used to filter out stray light. The transmitted light is measured with an InGaAs photo-detector. Finally, lock-in technique is used for noise reduction.

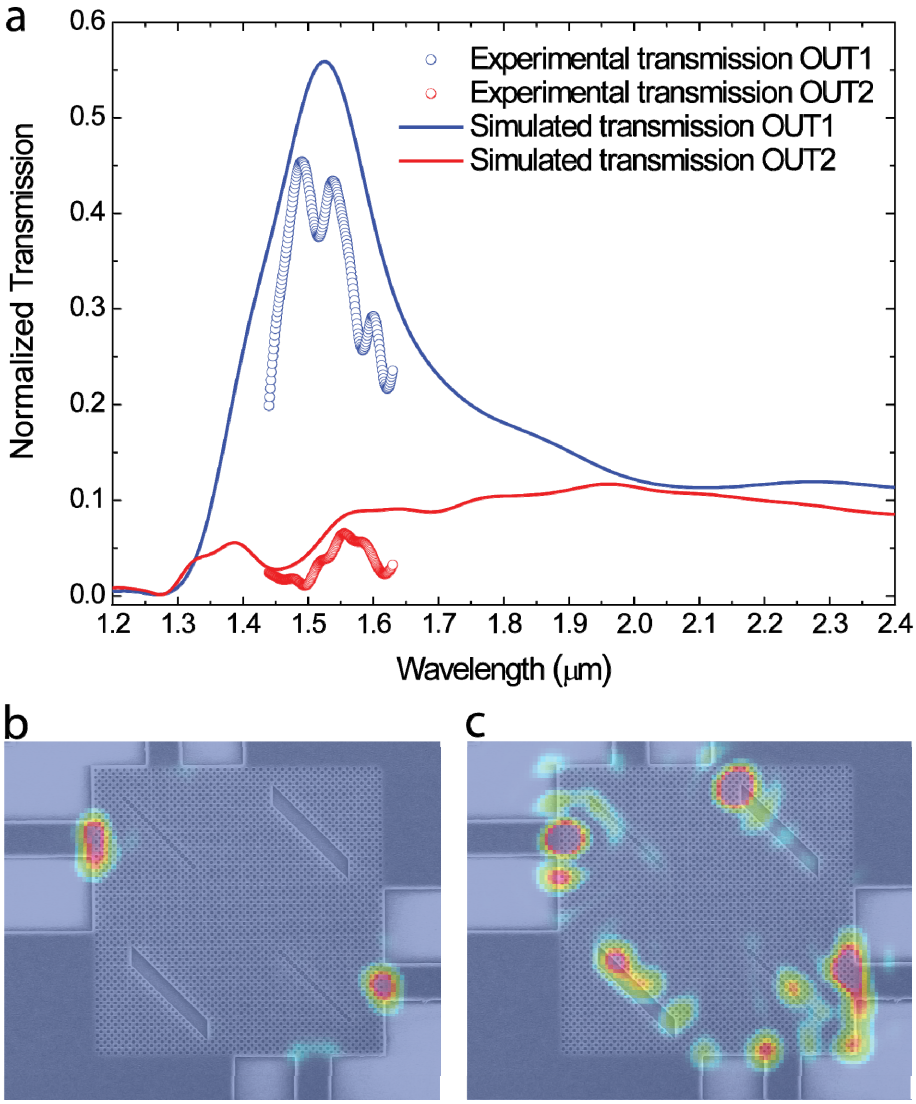


Figure 4. 4a, Comparison of measurements and simulations of transmission spectra. Blue and red circles are measurements at OUT1 and OUT2, respectively. Blue and red curves are FDTD simulations at OUT1 and OUT2, respectively. The green dash curve is the simulation of the vertical loss into air. 4b, Top-view observation of the MZI when light is propagating at 1.5 μm. This is the on-collimation case: only scattered light from the waveguide-PhC interfaces is observed. 4c, Top-view observation of the MZI when light is propagating at 1.62 μm. This is the off-collimation case: scattered light is observed at the waveguide-PhC interface as well as at the beam splitter and mirror structures. Note that the SEM images of the MZI in figure 4b and 4c are superimposed on the scattered light images from the optical microscope to guide the eye.

Downloaded from SPIE Digital Library on 19 Mar 2010 to 131.180.130.114. Terms of Use: http://spiedl.org/terms

We will discuss and compare the simulated unidirectional output behaviour of the MZI with the optical transmission measurement results. In figure 4a, the 3D finite-difference time-domain (FDTD) simulations for output spectra were plotted as blue and red lines in a wide wavelength range from 1.2 to 2.4 μm. From the normalized transmission spectrum at OUT1 (blue curve in figure 4a), a peak at 1.5 μm with a transmission of about 0.6 is observed, indicating the collimation region. Outside the collimation region, the beam propagating at longer wavelengths spreads out. Therefore, not all the transmitted light is collected at the output waveguides, resulting in a significantly weak transmission level of about 0.1. The ΓM stop gap of the PhC under study is observed for wavelengths lower than 1.3 μm, where the transmission level is almost zero. It is important to note that the shape of the OUT1 transmission spectrum originates not only from the optical density-of-state of the lowest energy band, but also from the diffraction and interference effect of this particular MZI structure. At the collimation wavelengths, the two collimated beams from different paths re-joined at S2 with a small spatial distribution. Thus, the interference effect is strong, resulting in a large difference between the output transmission levels. Outside the collimation region, the interference is so weak that the output signals are almost equal. The interesting point in the OUT2 output spectrum (red curve in figure 4a) is that although the transmission level outside the collimation region is low due to the diffraction effect, the transmission at the collimation region is even lower because of the destructive interference. These output spectra characteristic clearly shows that the collimation effect is crucial for the presence of the unidirectional output behaviour.

The measured transmission spectra for OUT1 and OUT2 output were depicted as blue and red circles, respectively. The large transmission-level difference between OUT1 and OUT2 at a wavelength of 1.5 μm confirms the unidirectional output behaviour, consistent with FDTD simulations. The spectra, which are peaked in OUT1 and minimum in OUT2 around 1.5 μm, implying a collimation regime, are also in agreement with simulations. Although the measured spectra are limited to the light source range (1.44-1.63 μm), they cover the collimation region and present the unidirectional output behaviour of the PhC MZI.

4.2. Out-of-plane loss simulation and far-field optical microscopic measurement

It is noted from both simulations and measurements that the addition of maximum transmission at the two outputs is only about 0.6. The total loss is attributed to mode mismatches at the waveguide-PhC interfaces, beam splitters and mirrors thus generating vertical leakage to air/SiO_2 cladding layers and back reflections. In practice, additional losses might also originate from fabrication imperfections, such as nanometer-scaled holes roughness or verticality.

The vertical observations of out-of-plane optical loss are made with a Navitar Zoom lens microscope with a 17-mm working distance Nikon 50x objective and a Xenics infrared camera (XEVA, 0.9 - 1.7 μm. The results are illustrated in figure 4b and 4c. Beam propagation along two MZI branches (S1M1S2, S1M2S2) is not visible in the top-view observations because of the good vertical confinement in the PhC slab. Figure 4b depicts the on-collimation case, where the collimated beams become vertically scattered only at waveguide-PhC interfaces. Two bright dots are observed at the waveguide-PhC interfaces of the input waveguide IN1 and the output waveguide OUT1, implying intense signals entering and exiting the MZI at the output waveguide OUT1. The less bright dot is observed at the waveguide-PhC interface of the output waveguide OUT2, implying a weak signal exiting the MZI at the output waveguide OUT2. Figure 4c depicts the off-collimation case, where the diffracted beams become vertically scattered at the waveguide-PhC interfaces as well as at the beam splitters and mirrors. The scattering becomes more visible at the waveguide-PhC interface of the output waveguide OUT2 compared to the on-collimation case in figure 4b, indicating a smaller output signal difference between OUT1 and OUT2. Although the propagations of diffracted and collimated beams were not observed, those evidences could be seen in the vertically scattering visibility at the off-collimation wavelength in contrast with the on-collimation wavelength. These top-view observations confirm the unidirectional output behaviour and present the low-loss property of the PhC MZI operating in the self-collimation mode.

5. OUTLOOK AND CONCLUSION

In terms of further developments and applications for this interferometer, an ultra-compact modulator for photonic integrated active silicon devices would be an obvious first choice. Active switching can be achieved by introducing a sufficient phase shift locally at the beam splitter S2, for instance, by making silicon suspended membrane and inserting high refractive index dielectric mesas into the air holes [16, 17]. In this way, optical active operations can be

Downloaded from SPIE Digital Library on 19 Mar 2010 to 131.180.130.114. Terms of Use: http://spiedl.org/terms

implemented in very small devices because, unlike in conventional waveguide based modulators, sufficient phase shifts are free from the interferometer arms' length requirement. Alternatively, a mechanical modulator can be made by utilizing the PhC MZI suspended membrane. By deflecting the membrane on one arm of the MZI while keeping the other arm fixed, one can expect a phase shift between the two arms, thus generating switching operations. The PhC MZI structure presented here is also promising for micro-mechanical sensor and lab-on-a-chip applications because the phase shifts, induced either locally at a beam splitter or along an interferometer arm, can be monitored as the differential output.

In summary, we have demonstrated the unidirectional output behaviour of the collimation silicon PhC MZI using the optical transmission spectroscopy and far-field optical microscopy. The pronounced contrast in the transmission level at 1.5 μm wavelength of the two outputs was observed, in agreement with the FDTD simulations. The output intensity contrast and evidences of the collimation effect were also observed in real space.

REFERENCES

1. Kirchain, R. and L. Kimerling, *A roadmap for nanophotonics.* Nature Photonics, 2007. **1**: p. 303-306.
2. Liu, A., et al., *High-speed optical modulation based on carrier depletion in a silicon waveguide.* Optics Express, 2008. **15**: p. 660-668.
3. Anderson, S.P., A.R. Schroff, and P.M. Fauchet, *Slow light with photonic crystal for on-chip optical interconnects.* Advances in Optical Technologies, 2008. **2008**(Article ID 293531).
4. Vlasov, Y.A., et al., *Active control of slow light on a chip with photonic crystal waveguides.* Nature, 2005. **438**: p. 65-69.
5. Mansouri-Birjandi, M.A., M.K. Moravvej-Farshi, and A. Rostami, *Ultrafast low-threshold all-optical switch implementater by arays of ring resonators coupled to a Mach-Zehnder interferometer arm: based on 2D photonic crystals.* Applied Optics, 2008. **47**: p. 5041-5050.
6. Rakich, P.T., et al., *Achieving centimeter-scale supercollimation in a large-area two-dimensional photonic crystal.* Nature Materials, 2006. **5**: p. 93-96.
7. Witzens, J., M. Loncar, and A. Scherer, *Self-collimation in planar photonic crystals.* IEEE J. Sel. Quantum Electron., 2002. **8**: p. 1246-1257.
8. Kosaka, H., et al., *Self-collimating phenomena in photonic crystals.* Applied Physics Letters, 1999. **74**: p. 1212-1215.
9. Prather, D.W., et al., *Self-collimation in photonic crystal structures: a new paradigm for applications and device development.* J. Phys. D: Appl. Phys., 2007. **40**: p. 2635-2651.
10. Prather, D.W., et al., *Dispersion-based optical routing in photonic crystal.* Optics Letters, 2004. **29**: p. 50-52.
11. Lee, S.-G., et al., *Line defect induced bending and splitting of self-collimated beams in two-dimentional photonic crystals.* Applied Physics Letters, 2005. **87**: p. 118106.
12. Yu, X. and S. Fan, *Bends and splitters for selft-collimated beams in photonic crystals.* Applied Physics Letters, 2003. **83**: p. 3251-3253.
13. Ramaswami, R. and K.N. Sivarajan, *Optical networks: A pratical perspective*. 1998, San Francisco: Morgan Kaufmann.
14. Zhao, D., et al., *Photonic crystal Mach-Zehnder interferometer based on self-collimation.* Applied Physics Letters, 2007. **90**: p. 231114.
15. Caro, J., et al., *Transmission measurement of the photonic band gap of GaN photonic crystal slabs.* Applied Physics Letters, 2008. **93**: p. 051117-051119.
16. Takahata, T., et al. in *Proceedings of MEMS 2006*. 2006. Instanbul, Turkey.
17. Zhou, W., et al., *Novel reconfigurable semiconductor photonic crystal-MEMS device.* Solid-state electronics, 2006. **50**: p. 908-913.

Downloaded from SPIE Digital Library on 19 Mar 2010 to 131.180.130.114. Terms of Use: http://spiedl.org/terms